

Loop induced top quark FCNC through top quark and dark matter interactions

Yandong Liu^{a,b} Bin Yan^c Rui Zhang^d

^aKey Laboratory of Beam Technology of Ministry of Education, College of Nuclear Science and Technology, Beijing Normal University, Beijing 100875, China

^bBeijing Radiation Center, Beijing 100875, China

^cTheoretical Division, Group T-2, MS B283, Los Alamos National Laboratory, P.O. Box 1663, Los Alamos, NM 87545, USA

^dTheoretical Physics Division, Institute of High Energy Physics, Beijing 100049, China

E-mail: ydliu@bnu.edu.cn, binyan@lanl.gov, zhangr@ihep.ac.cn

ABSTRACT: We present a comprehensive analysis of the loop induced top quark FCNC signals at the LHC within one class of the simplified model. The loop level FCNC interactions are well motivated to avoid the hierarchy of the top quark couplings from the new physics and standard model. Such a theory will posit a Majorana dark matter candidate and could be tested through dark matter relic density, direct detection experiments (the scattering between dark matter and heavy nuclei), and the collider signals at the LHC. We find that the spin-independent (SI) scattering between Majorana dark matter and nuclei will vanish at the leading order, while the next-to-leading order correction to the SI scattering becomes significance to constrain the parameter space of the model. A detailed comparison from direct detection experiments and LHC searches is also discussed and both of them are very important to full constrain the model.

Contents

1	Introduction	1
2	Model Setup	3
3	Loop induced top quark FCNC	4
4	Dark Matter	7
4.1	relic density	8
4.2	direct detection	10
5	Direct Search at the LHC	15
6	Conclusion	16
A	Feynman Integral	17

1 Introduction

Top quark flavor changing neutral current (FCNC) processes can only occur via loops in the standard model (SM) and their production rates are highly suppressed by the Glashow-Iliopoulos-Maiiani mechanism [1]. The branching ratios of top quark decay $t \rightarrow Xq$, where $X = h, Z, \gamma, g$ and $q = u, c$ are around $10^{-16} \sim 10^{-12}$ in the SM [2]. As a result, it would be a challenge to observe the SM top quark FCNC effects at the current or foreseeable dataset. However, a large top quark FCNC signals could be induced in the new physics (NP) beyond the SM at the tree or loop level, e.g. $\text{BR}(t \rightarrow Xq) \sim \mathcal{O}(10^{-5})$ in the minimal supersymmetry standard model (MSSM) [2] or two Higgs doublet model [3–5]. Therefore, any evidence of the top quark FCNC signals would shed light on the various possible NP models and also the underlying mechanism of generating top quark FCNC.

The top quark FCNC effects have been extensively studied by the theoretical [6–19] and experimental [20–35] groups within the SM effective field theory (SMEFT) framework or specific NP models. Both the ATLAS and CMS collaborations show that the current dataset could give a strong constraint on the $\text{BR}(t \rightarrow Xq)$ through top quark rare decay and single top quark production. For example, the most stringent limits on the branching ratios of $\text{BR}(t \rightarrow \gamma u) < 6.1 \times 10^{-5}$ and $\text{BR}(t \rightarrow \gamma c) < 2.2 \times 10^{-4}$ at the 95% confidence level (CL) set by the 13 TeV single top quark and a photon production [21]. The limits for the $\text{BR}(t \rightarrow gq)$ is comparable to the $\text{BR}(t \rightarrow \gamma q)$ and it shows that the upper limits are 2×10^{-5} and 2×10^{-4} for u and c quark, respectively at the LHC Run-I [23, 24]. Both

the top quark decay [23, 24, 33, 35] and single top quark associated with a gauge boson production [28, 34] could constrain the branching ratios $\text{BR}(t \rightarrow Z/hq)$ and the limits are dominated by the top quark decay, i.e. $\text{BR}(t \rightarrow Zu) < 1.7 \times 10^{-4}$, $\text{BR}(t \rightarrow Zc) < 2.4 \times 10^{-4}$, $\text{BR}(t \rightarrow hu) < 1.1 \times 10^{-3}$ and $\text{BR}(t \rightarrow hc) < 1.2 \times 10^{-3}$.

The SMEFT is a powerful framework to parametrize potential NP effects and are widely applied in the top quark FCNC phenomenology [36–38]. The Wilson coefficients are constrained to be around $\mathcal{O}(10^{-3}) \sim \mathcal{O}(10^{-2})$ with the NP scale $\Lambda = 1$ TeV. With higher luminosity data being accumulated, an order of magnitude improvement on the top quark FCNC anomalous couplings are expected at the high-luminosity LHC (HL-LHC), operating at the $\sqrt{s} = 14$ TeV with an integrated luminosity of 3 ab^{-1} . It is thus timely to study what kind of NP (beyond the SMEFT) could induce the top quark FCNC anomalous couplings.

The top quark FCNC anomalous couplings could be generated through the tree or loop level in NP models. It is well know that the multiplet Higgs models could generate tree level top quark FCNC couplings if the Yukawa structure satisfies the Glashow-Weinberg-Paschos (GWP) theorem [39, 40], e.g. the general two Higgs double models. However, such models have been constrained seriously by top quark FCNC data, and, as a result a large hierarchy generated between top quark FCNC and other top quark couplings (e.g. tbW [41, 42] and $Zt\bar{t}$ [43]). This situation could be relaxed or avoided if we require the top quark FCNC couplings to be generated only in the loop level, which is similar to the case of the loop induced neutrino mass models [44, 45]. For example, the top quark FCNC couplings could be generated by triangle loop diagram through the squarks mixing effects in the MSSM and its value agrees well with the LHC limitation as well the mass scale of $\mathcal{O}(1)$ TeV for the heavy particles in the loop, without unduly small NP couplings.

One obvious way of generating loop induced top quark FCNC couplings is introducing an additional \mathcal{Z}_2 symmetry to avoid possible tree level interactions, i.e. new heavy particles are odd under the \mathcal{Z}_2 , while the SM particles are even. One byproduct of such models is that the lightest \mathcal{Z}_2 odd neutral particle could be a promising dark matter (DM) candidate. Therefore, it is useful to combine dark matter detection and the collider searches to constrain or search this kind of the NP models. Comparing to the UV complete theories such as MSSM, we would like to use a simplified model to show the idea in this work. The simplified models include a finite number of parameters with a reasonable simple theoretical framework and have become a robust mechanism to search various NP particles. In this work, we will focus on fermionic dark matter and scalar mediators. It is also possible to introduce a dark gauge boson in the loop, however, which is beyond the scope of this work. We show that the simplified model could generate the sizable top quark FCNC anomalous couplings and their predictions are consistent with the present LHC data and could be tested at the HL-LHC and future hadron colliders. In addition, the parameter space is also testable by the future dark matter direct detection experiments, (e.g. XENON20T [46] and DARWIN [47]) and dark matter searches at the LHC.

2 Model Setup

In this section, we discuss the detail of our simplified model. It contains a fermionic dark matter (χ) and scalar mediator particles which interact with the dark matter and the SM quarks. The dark matter is a singlet under the SM gauge groups and can be either a Dirac or a Majorana fermion and we will focus on Majorana case in this work. In general, the top quark could be left or right-handed under the $SU(2)_L$ gauge symmetry. However, the left-handed top and bottom quarks transform as doublet under $SU(2)_L$, and, as a result, any modification to the left-handed top quark couplings will also induce the correction to the B physics, e.g. [48, 49]. Therefore, we will focus on the right-handed top quark in order to avoid the possible constraints from precise measurements of B physics. The gauge representations of the mediators under the SM gauge groups $SU(3)_C \otimes SU(2)_L \otimes U(1)_Y$ are,

$$\Phi_1 \sim (3, 1, 2/3), \quad \Phi_2 \sim (3, 2, 1/6). \quad (2.1)$$

The gauge invariant Lagrangian in our model is,

$$\begin{aligned} \mathcal{L}_{\text{eff}} \supset & (D_\mu \Phi_1)^\dagger (D^\mu \Phi_1) - M_1^2 \Phi_1^\dagger \Phi_1 + (D_\mu \Phi_2)^\dagger (D^\mu \Phi_2) - M_2^2 \Phi_2^\dagger \Phi_2 \\ & + \frac{1}{2} \bar{\chi} (\not{\partial} - m_\chi) \chi + (y_t \bar{\chi} P_R t \Phi_1^* + y_u \bar{q}_u P_R \chi \Phi_2 + \text{h.c.}) - (\mu \Phi_1^* H \Phi_2 + \text{h.c.}), \end{aligned} \quad (2.2)$$

where H is the Higgs doublet field and defined as $H^T = \frac{1}{\sqrt{2}}(0, v + h)$ with $v = 246$ GeV in the unitarity gauge. The fields t and $q_u^T = (u, d)$ are the right-handed top quark and left-handed first generation quarks, respectively. It is straightforward to generalize our results to the second generation light quarks. A similar simplified model with other assumptions are also widely discussed in the literature and could be found in Refs. [50–52]. The covariant derivative in Eq. 2.2 is defined as,

$$D_\mu = \partial_\mu - ig_s G_\mu^a T^a - ig W_\mu^i \tau^i - ig' Y B_\mu. \quad (2.3)$$

Here G_μ^a , W_μ^i and B_μ are the $SU(3)_c$, $SU(2)_L$ and $U(1)_Y$ gauge fields, respectively, and g_s , g and g' are their gauge couplings. The gauge parameters g and g' are related to the electric charge and the Weinberg mixing angle by $g s_W = g' c_W = e$, where $s_W = \sin \theta_W$ and $c_W = \cos \theta_W$. Furthermore, T^a and τ^i are the $SU(3)_c$ and $SU(2)_L$ generators and Y is the hypercharge, in the representation of the field on which the derivative acts.

After the electroweak symmetry breaking, the colored doublet scalar $\Phi_2^T = (\phi_u, \phi_d)$ will mix with Φ_1 through the 3-scalar interaction. We define the mass eigenstates as ϕ_1, ϕ_2 and they could translate to the gauge eigenstates by

$$\begin{pmatrix} \phi_1 \\ \phi_2 \end{pmatrix} = \begin{pmatrix} \cos \theta & -\sin \theta \\ \sin \theta & \cos \theta \end{pmatrix} \begin{pmatrix} \Phi_1 \\ \phi_u \end{pmatrix}. \quad (2.4)$$

The mixing angle θ is defined as

$$\sin 2\theta = \frac{\sqrt{2}\mu v}{m_2^2 - m_1^2}, \quad (2.5)$$

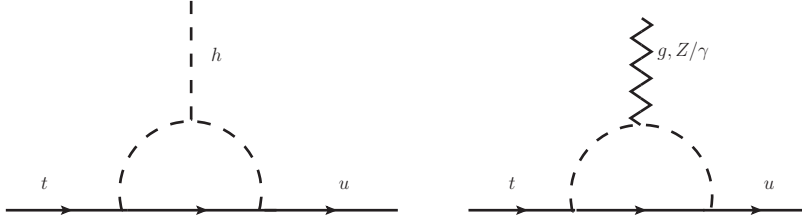


Figure 1. Illustrative one-loop Feynman diagrams to generate top quark FCNC anomalous couplings.

where $m_{1,2}$ are the mass of the two physics scalars,

$$m_1^2 = \frac{1}{2}(M_1^2 + M_2^2 - \sqrt{(M_1^2 - M_2^2)^2 + 2\mu^2 v^2}), \quad (2.6)$$

$$m_2^2 = \frac{1}{2}(M_1^2 + M_2^2 + \sqrt{(M_1^2 - M_2^2)^2 + 2\mu^2 v^2}). \quad (2.7)$$

3 Loop induced top quark FCNC

The top quark FCNC anomalous couplings could be generated through the triangle diagram in our simplified model, see Fig. 1 and the interactions can be parameterized by the effective operators under the $SU(3)_C \otimes U(1)_{EM}$,

$$\begin{aligned} \mathcal{L}_{\text{eff}} = & \lambda_{tqh} \bar{q}_L t_R h + \frac{\lambda_{tq\gamma}}{m_t} \bar{q}_L \sigma_{\mu\nu} t_R A^{\mu\nu} + \frac{\lambda_{tqg}}{m_t} \bar{q}_L \sigma_{\mu\nu} t_R G^{a\mu\nu} T^a \\ & + \frac{\lambda_{tqZ}^{(1)}}{m_t} \bar{q}_L \sigma_{\mu\nu} t_R Z^{\mu\nu} + \lambda_{tqZ}^{(2)} \bar{q}_L \gamma_\mu t_L Z^\mu + h.c. \end{aligned} \quad (3.1)$$

Note that the gauge invariance of $U(1)_{EM}$ forbids the vector and axial-vector current interactions of $tq\gamma$ and tqg . The matching coefficients could be got from one-loop calculation and

the results are,

$$\lambda_{tqh} = \frac{y_t y_u m_\chi}{16\sqrt{2}\pi^2} \left\{ \frac{\sin 2\theta}{\sqrt{2}v} (B_{\chi 1}^0 - B_{\chi 2}^0) + \mu (\sin^4 \theta - \sin^2 \theta \cos^2 \theta) C_{\chi 12}^{0ht} + \right. \\ \left. \mu (\cos^4 \theta - \sin^2 \theta \cos^2 \theta) C_{\chi 21}^{0ht} + 2\mu \sin^2 \theta \cos^2 \theta C_{\chi 11}^{0ht} + 2\mu \sin^2 \theta \cos^2 \theta C_{\chi 22}^{0ht} \right\}, \quad (3.2)$$

$$\lambda_{tq\gamma} = \frac{Qe}{32\pi^2} \frac{m_\chi}{m_t} y_t y_u \sin \theta \cos \theta (B_{\chi 2}^t - B_{\chi 2}^0 - B_{\chi 1}^t + B_{\chi 1}^0), \quad (3.3)$$

$$\lambda_{tqg} = \frac{g_s}{32\pi^2} \frac{m_\chi}{m_t} y_t y_u \sin \theta \cos \theta (B_{\chi 2}^t - B_{\chi 2}^0 - B_{\chi 1}^t + B_{\chi 1}^0), \quad (3.4)$$

$$\lambda_{tqZ}^{(1)} = \frac{g}{16\pi^2 c_W} \frac{m_\chi m_t}{4(m_t^2 - m_Z^2)} y_t y_u \sin 2\theta \left\{ (B_{\chi 1}^0 - B_{\chi 2}^0) f_R - \frac{m_t^2 + m_Z^2}{m_t^2 - m_Z^2} f_L (B_{\chi 1}^t - B_{\chi 2}^t) \right. \\ \left. + \frac{m_Z^2}{m_t^2 - m_Z^2} [(2f_L - \cos^2 \theta) B_{11}^Z - (2f_L - \sin^2 \theta) B_{22}^Z + \cos 2\theta B_{12}^Z] \right. \\ \left. + \frac{m_Z^2}{2(m_t^2 - m_Z^2)} [(2f_L - \cos^2 \theta) \lambda(m_1) C_{1\chi 1}^{0tZ} - (2f_L - \sin^2 \theta) \lambda(m_2) C_{2\chi 2}^{0tZ}] \right. \\ \left. + \frac{\cos^2 \theta}{4(m_t^2 - m_Z^2)} [2(m_1^2 - m_2^2) m_t^2 + (\lambda(m_1) + \lambda(m_2)) m_Z^2] C_{2\chi 1}^{0tZ} \right. \\ \left. + \frac{\sin^2 \theta}{4(m_t^2 - m_Z^2)} [2(m_1^2 - m_2^2) m_t^2 - (\lambda(m_1) + \lambda(m_2)) m_Z^2] C_{1\chi 2}^{0tZ} \right\} \quad (3.5)$$

$$\lambda_{tqZ}^{(2)} = -\frac{g}{16\pi^2 c_W} \frac{m_\chi}{m_t} y_t y_u f_L \sin \theta \cos \theta (B_{\chi 2}^t - B_{\chi 2}^0 - B_{\chi 1}^t + B_{\chi 1}^0) + 2\lambda_{tqZ}^{(1)}. \quad (3.6)$$

where

$$f_L = \frac{1}{2} - \frac{2}{3} s_W^2, \quad f_R = -\frac{2}{3} s_W^2, \quad \lambda(m_i) = 2m_\chi^2 - 2m_i^2 - m_t^2 + m_Z^2. \quad (3.7)$$

We abbreviate the scalar functions as $B_{ij}^a = B_0(m_a^2, m_i^2, m_j^2)$ and $C_{ijk}^{abc} = C_0(m_a^2, m_b^2, m_c^2, m_i^2, m_j^2, m_k^2)$, and their definitions can be found in Ref. [53]. Note that $m_{a,b,c} = 0$ for $a, b, c = 0$.

In the limit of $m_{1,2,\chi} \sim \Lambda \gg m_{t,h,Z}$, the matching coefficients could be simplified as,

$$\lambda_{tqh} = -\frac{1}{384\sqrt{2}\pi^2} y_t y_u \mu \frac{m_t^2}{\Lambda^3}, \quad (3.8)$$

$$\lambda_{tq\gamma} = \frac{iQe}{392\sqrt{2}\pi^2} y_t y_u \frac{\mu v m_t}{\Lambda^3}, \quad (3.9)$$

$$\lambda_{tqg} = \frac{ig_s}{392\sqrt{2}\pi^2} y_t y_u \frac{\mu v m_t}{\Lambda^3}, \quad (3.10)$$

$$\lambda_{tqZ}^{(1)} = -\frac{g y_t y_u (f_L + f_R)}{768\sqrt{2}\pi^2 c_W} \frac{\mu v m_t}{\Lambda^3}, \quad (3.11)$$

$$\lambda_{tqZ}^{(2)} = \frac{g y_t y_u (f_L - f_R)}{384\sqrt{2}\pi^2 c_W} \frac{\mu v m_t}{\Lambda^3}. \quad (3.12)$$

We should note that the scale $\mu \sim v$ in above limit, see Eq. 2.5. It is also worth noting that a large μ could be generated from the large mass splitting between ϕ_1 and ϕ_2 for a fixed

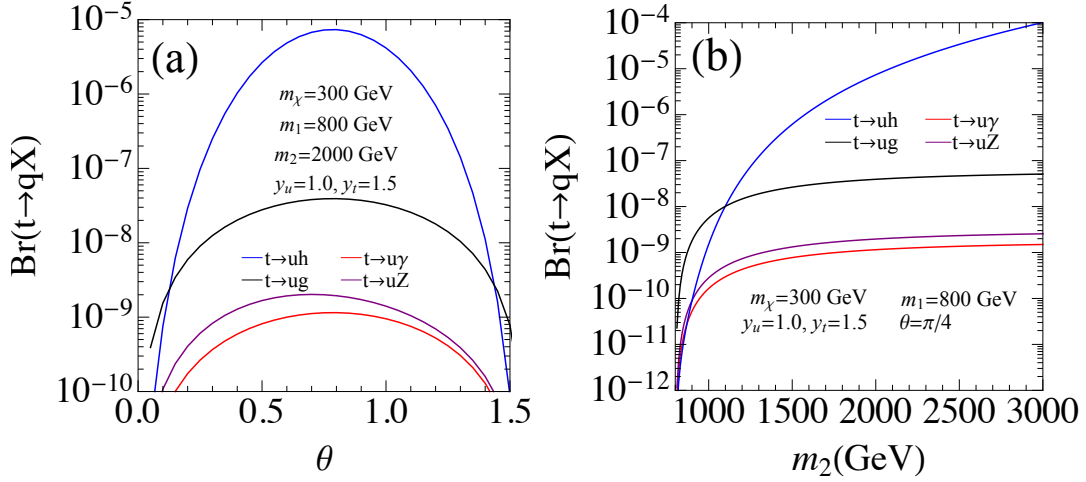


Figure 2. The top quark FCNC decay branching ratios in our simplified model.

mixing angle θ . In that case, the tqh anomalous coupling will be enhanced by the triple scalar interactions, see the coupling in the limit of $m_2 \gg m_{1,\chi} \sim m_{t,h,Z}$,

$$\lambda_{tqh} = -\frac{13y_u y_t m_2^2 \sin^3 2\theta}{1536\pi^2 m_\chi v}. \quad (3.13)$$

The partial decay widths of top quark through the FCNC anomalous couplings are,

$$\Gamma(t \rightarrow qh) = \lambda_{tqh}^2 \frac{m_t}{32\pi} \left(1 - \frac{m_h^2}{m_t^2}\right)^2, \quad (3.14)$$

$$\Gamma(t \rightarrow q\gamma) = \lambda_{tq\gamma}^2 \frac{m_t}{4\pi}, \quad (3.15)$$

$$\Gamma(t \rightarrow qg) = \lambda_{tqg}^2 \frac{m_t}{4\pi} 4C_F, \quad (3.16)$$

$$\Gamma(t \rightarrow qZ) = \frac{m_t}{32\pi} \left(1 - \frac{m_Z^2}{m_t^2}\right)^2 \left[4 \left(\lambda_{tqZ}^{(1)}\right)^2 \left(2 + \frac{m_Z^2}{m_t^2}\right) - 12\lambda_{tqZ}^{(1)}\lambda_{tqZ}^{(2)} + \left(\lambda_{tqZ}^{(2)}\right)^2 \left(2 + \frac{m_Z^2}{m_t^2}\right)\right]. \quad (3.17)$$

In the limit of $m_{1,2,\chi} \sim \text{TeV} \gg m_{t,h,Z}$, the largest branching ratio is from $t \rightarrow qg$, i.e. $\text{BR}(t \rightarrow qg) \sim \mathcal{O}(10^{-9})$, however, it is out of reach for the HL-LHC [54]. While the branching ratio of $t \rightarrow qh$ could be enhanced by the scale μ when $m_2 \gg m_1$ (see Eq. 3.13), as a consequence, the $t \rightarrow qh$ would be a promising channel to search the top quark FCNC in our model.

Figure 2 shows the decay branching ratios from the top quark FCNC anomalous couplings with the benchmark parameters. The LoopTools package is used in our numerical calculation [55]. It shows that the branching ratios will reach the maximal when the mixing angle $\theta \sim \pi/4$ and the typical branching ratios of $t \rightarrow q + Z/\gamma/g$ are around $\mathcal{O}(10^{-9}) - \mathcal{O}(10^{-8})$. However, the $\text{BR}(t \rightarrow qh)$ could be reached around $\mathcal{O}(10^{-5})$ when $m_2 \gg m_1$, which is large

enough and can be detected at the HL-LHC and future hadron colliders. We summarize the allowed parameter space on the plane of m_1 and m_2 at the 95% C.L. from the HL-LHC (red) [56, 57], HE-LHC (blue) [58] and FCC-HH (gray) [58] in Fig. 3.

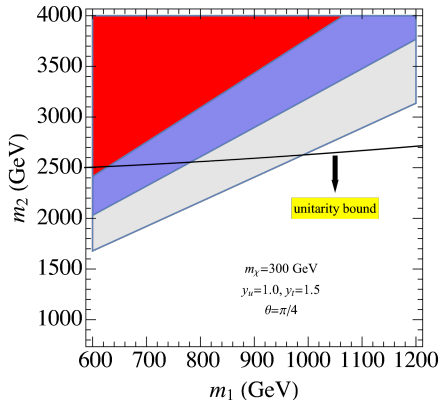


Figure 3. The expected sensitivity to the model parameters through $t \rightarrow qh$ from the HL-LHC (red), HE-LHC (blue) and FCC-HH (gray) at 95% C.L.. The black line denotes the unitarity bound from the scattering $\phi_i \phi_j^* \rightarrow W_L^+ W_L^-$.

We notice that the scale μ will be constrained by the unitarity of the scattering $\phi_i \phi_j^* \rightarrow W_L^+ W_L^-$ ($i, j = 1, 2$), with longitudinal polarized W boson. Based on the analysis of the partial wave expansion [59], for the s -wave,

$$a = \frac{1}{64\pi^2} \int d\Omega \mathcal{M}(\phi_i \phi_j^* \rightarrow W_L W_L), \quad (3.18)$$

and the coupled matrix is

$$a = \begin{pmatrix} 0 & \frac{\sqrt{2}\mu\delta_{i,j}}{32\pi v} \\ -\frac{\sqrt{2}\mu\delta_{i,j}}{32\pi v} & 0 \end{pmatrix}, \quad (3.19)$$

where $\delta_{i,j}$ is the color index. The unitarity of the scattering amplitude requires that the absolute value of the eigenvalues from above coupled matrix should be small than 1 [59–62]. Therefore, the upper limit of μ is,

$$|\mu| \lesssim 17 \text{ TeV}. \quad (3.20)$$

We can also translate the upper limit of μ to the mass splitting between ϕ_1 and ϕ_2 through Eq. 2.5; see the black line in Fig. 3. We should note that the unitarity bound would be stronger than the HL-LHC.

4 Dark Matter

In this section we discuss the constraints from the DM relic abundance and the direct detection experiments to our simplified model.

4.1 relic density

The DM relic abundance has been measured by Planck with a high accuracy, i.e. $\Omega_\chi h^2 = 0.1200 \pm 0.0012$ [63]. It requires that the theoretical predicted relic abundance from the simplified model should be smaller than the observed value to avoid dark matter overproduction. Assuming DM particle is thermally produced in the early universe, $\Omega_\chi h^2$ is totally determined by the thermally averaged annihilation cross sections $\langle\sigma v_{\text{rel}}\rangle$. The evaluation of DM density is controlled by the Boltzmann equation and its relic abundance is given by

$$\Omega_\chi h^2 \approx 2.76 \times 10^8 Y \frac{m_\chi}{\text{GeV}}, \quad (4.1)$$

where Y is the DM number density of today in the comoving frame,

$$Y = \sqrt{\frac{45}{\pi}} \frac{g_*(x_f)^{1/2}/g_{*s}(x_f)}{m_{\text{PL}} m_\chi \langle\sigma v_{\text{rel}}\rangle} x_f. \quad (4.2)$$

Here $x_f \equiv m_\chi/T_f$, with T_f denoting the decoupling temperature, m_{PL} is the Planck mass. $g_*(x_f)$ and $g_{*s}(x_f)$ are the effective energy and entropy degrees of freedom at the temperature of DM decoupling, respectively. Therefore, the minimal of the $\langle\sigma v_{\text{rel}}\rangle$ should be,

$$\langle\sigma v_{\text{rel}}\rangle \approx 0.71 \frac{0.12}{\Omega_\chi h^2} \frac{x_f g_*(x_f)^{1/2}/g_{*s}(x_f)}{25 \cdot 0.1} \text{ pb}. \quad (4.3)$$

The annihilation cross section can be expanded based on the velocity, i.e. $\langle\sigma v_{\text{rel}}\rangle \doteq a + b\langle v_{\text{rel}}^2\rangle + \mathcal{O}(\langle v_{\text{rel}}^4\rangle)$. The coefficients a and b describe the contributions from s-wave and p-wave scattering, respectively. Since $\langle v_{\text{rel}}^2\rangle \sim 0.3$ during the DM decoupling, the s-wave scattering will play the key role for the DM annihilation.

The dominant contributions to DM annihilation come from $t\bar{t}$, $t\bar{u}$ and $u\bar{t}$ final states through s-wave production and $u\bar{u}$, $d\bar{d}$ modes from p-wave scattering; see Fig. 4. The s-wave contributions from $u\bar{u}$ and $d\bar{d}$ will be suppressed by the quark mass due to the flip of the quark helicity and can be ignored in the analysis. The annihilation cross sections are given by,

$$\langle\sigma v_{\text{rel}}\rangle_{t\bar{t}} \simeq \frac{N_C y_t^4 m_t^2 (2m_\chi^2 + (m_2^2 - m_1^2) \cos(2\theta) + m_1^2 + m_2^2 - 2m_t^2)^2}{128\pi (m_\chi^2 + m_1^2 - m_t^2)^2 (m_\chi^2 + m_2^2 - m_t^2)^2} \sqrt{1 - \frac{m_t^2}{m_\chi^2}}, \quad (4.4)$$

$$\langle\sigma v_{\text{rel}}\rangle_{t\bar{u}+u\bar{t}} \simeq \frac{N_C y_t^2 y_u^2 m_\chi^2 (m_1^2 - m_2^2)^2 \sin^2(2\theta)}{2\pi (2m_\chi^2 + 2m_1^2 - m_t^2)^2 (2m_\chi^2 + 2m_2^2 - m_t^2)^2} \left(1 - \frac{m_t^2}{4m_\chi^2}\right)^2, \quad (4.5)$$

$$\begin{aligned} \langle\sigma v_{\text{rel}}\rangle_{u\bar{u}} \simeq & \frac{y_u^4}{64\pi (m_\chi^2 + m_1^2)^4 (m_\chi^2 + m_2^2)^4} \{m_\chi^2 m_1^4 m_2^4 \Delta^2 + 8m_\chi^4 m_1^4 m_2^4 \Delta \\ & + m_\chi^6 [(m_1^4 + m_2^4) \Delta^2 + 20m_1^4 m_2^4] + 4m_\chi^8 [(m_1^2 + m_2^2) \Delta^2 + 4m_1^2 m_2^2 (m_2^2 - m_1^2) \cos(2\theta)] \\ & + m_\chi^{10} [5\Delta^2 + 4(m_1^4 + m_2^4)] + 8m_\chi^{12} \Delta + 4m_\chi^{14}\} v_{\text{rel}}^2, \end{aligned} \quad (4.6)$$

$$\langle\sigma v_{\text{rel}}\rangle_{d\bar{d}} \simeq \frac{y_u^4 m_\chi^2 (m_\chi^4 + M_2^4)}{16\pi (m_\chi^2 + M_2^2)^4} v_{\text{rel}}^2, \quad (4.7)$$

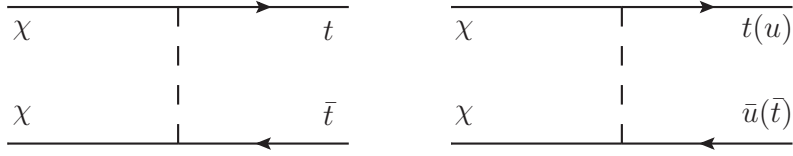


Figure 4. Majorana dark matter annihilation processes.

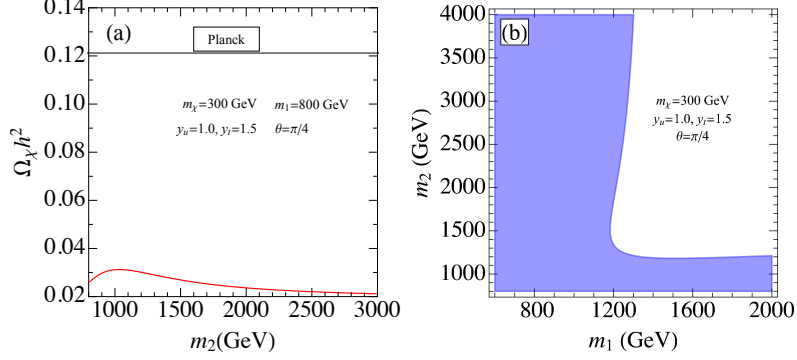


Figure 5. Dark matter relic abundance and limits from Planck 2018 [63]

where $N_C = 3$ denotes the color factor of quarks and $\Delta = m_1^2 + m_2^2 - (m_2^2 - m_1^2) \cos(2\theta)$. As we expected that the annihilation from $t\bar{t}$ mode contributes to the s-wave and the rate is proportional to m_t due to the flip of the quark helicity, while $u\bar{u}$ and $d\bar{d}$ modes will only contribute to the p-wave when we ignore their mass. Furthermore, the scattering from $t\bar{u}$ and $u\bar{t}$ final states come from the mixing between the scalars Φ_1 and Φ_2 . As a result, the annihilation rates to $t\bar{u}$ and $u\bar{t}$ are proportional to the mixing angle $\sin(2\theta)$.

In Fig. 5(a), we show the relic density in our simplified model with the benchmark parameters $m_\chi = 300$ GeV, $m_1 = 800$ GeV, $y_u = 1$, $y_t = 1.5$ and $\theta = \pi/4$. The black line represents the upper limit from Planck 2018 at the 68% C.L. [63]. We note that the relic density approaches a constant in the large m_2 region due to the decoupling behavior of ϕ_2 . Its effects could be understood from the thermal cross sections $\langle\sigma v_{\text{rel}}\rangle_{t\bar{u}+u\bar{t}}$ and $\langle\sigma v_{\text{rel}}\rangle_{t\bar{t}}$ in the limit of $m_2 \rightarrow \infty$,

$$\langle\sigma v_{\text{rel}}\rangle_{t\bar{t}} \simeq \frac{N_C y_t^4 m_t^2 (1 + \cos(2\theta))^2}{128\pi (m_1 + m_\chi - m_t)^2} \sqrt{1 - m_t^2/m_\chi^2} + \mathcal{O}(1/m_2^2), \quad (4.8)$$

$$\langle\sigma v_{\text{rel}}\rangle_{t\bar{u}+u\bar{t}} \simeq \frac{N_C y_t^2 y_u^2 m_\chi^2 \sin^2(2\theta)}{8\pi (2m_1^2 + 2m_\chi^2 - m_t^2)^2} \sqrt{1 - m_t^2/4m_\chi^2} + \mathcal{O}(1/m_2^2). \quad (4.9)$$

In Fig. 5(b), we show the allowed parameter space on the plane of m_1 and m_2 . This analysis shows that the limits from relic abundance measurement should be weak to our model parameters.

4.2 direct detection

Direct detection is one of cornerstones of DM searches. The goal of the experiments is to detect the rare scattering between the non-relativistic DM and the target material; see Fig. 6. The scattering cross sections could be separated into spin-independent (SI) and spin-dependent (SD) contributions based on the interactions between DM and SM particles. Since the SI scattering resolves the entire nucleus coherently, the cross section will be enhanced by the squared number of scattering centers (nucleons). While for the SD scattering, DM couples to the nucleon spin and the coherent enhancement effects will disappear. To describe the SI and SD scatterings, we use the following effective Lagrangian [64, 65],

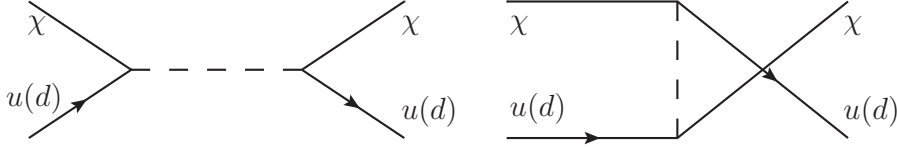


Figure 6. DM direct detection process at the tree level.

$$\mathcal{L} = \sum_{u,d} f_q^{\text{SD}} \bar{\chi} \gamma^\mu \gamma^5 \chi \bar{q} \gamma_\mu \gamma^5 q + \sum_{u,d,s} \mathcal{L}_q^{\text{EFT}} + \mathcal{L}_g^{\text{EFT}}, \quad (4.10)$$

where

$$\mathcal{L}_q^{\text{EFT}} = f_q m_q \bar{\chi} \chi \bar{q} q + \frac{g_q^{(1)}}{2m_\chi} \bar{\chi} i(\partial^\mu \gamma^\nu + \partial^\nu \gamma^\mu) \chi O_{q,\mu\nu}^{(2)} + \frac{g_q^{(2)}}{m_\chi^2} \bar{\chi} (i\partial^\mu) (i\partial^\nu) \chi O_{q,\mu\nu}^{(2)}, \quad (4.11)$$

$$\mathcal{L}_g^{\text{EFT}} = f_G \bar{\chi} \chi G_{\mu\nu}^a G^{a\mu\nu} + \frac{g_G^{(1)}}{2m_\chi} \bar{\chi} i(\partial^\mu \gamma^\nu + \partial^\nu \gamma^\mu) \chi O_{G,\mu\nu}^{(2)} + \frac{g_G^{(2)}}{m_\chi^2} \bar{\chi} (i\partial^\mu) (i\partial^\nu) \chi O_{G,\mu\nu}^{(2)}. \quad (4.12)$$

The twist-2 operators $O_{q,\mu\nu}^{(2)}$ and $O_{G,\mu\nu}^{(2)}$ are defined as,

$$O_{q,\mu\nu}^{(2)} \equiv \frac{1}{2} \bar{q} (\gamma^{\{\mu} iD_-^{\nu\}} - \frac{g^{\mu\nu}}{4} i\not{D}), \quad (4.13)$$

$$O_{G,\mu\nu}^{(2)} \equiv -G^{a\mu\lambda} G_{\lambda\nu}^a + \frac{g^{\mu\nu}}{4} (G_{\alpha\beta}^a)^2. \quad (4.14)$$

Here,

$$\gamma^{\{\mu} iD_-^{\nu\}} = \frac{1}{2} i(\gamma^\mu D_-^\nu + D_-^\mu \gamma^\nu), \quad D_-^\mu = D^\mu - \overleftarrow{D}^\mu. \quad (4.15)$$

The Wilson coefficients f_q^{SD} , f_j and $g_j^{(i)}$ with $j = q, G$ and $i = 1, 2$ could match to our simplified model. It is clear that f_q^{SD} term describes the SD scattering, while $\mathcal{L}_q^{\text{EFT}}$ and $\mathcal{L}_g^{\text{EFT}}$ contribute to SI process. The matrix element of DM SD scattering with a nucleon target ($N = p$ or n) is,

$$f^{\text{SD}} = \sum_{u,d} f_q^{\text{SD}} \Delta_N^q. \quad (4.16)$$

The hadronic matrix element Δ_N^q is defined through,

$$\langle N | \bar{q} \gamma^\mu \gamma^5 q | N \rangle = 2s^\mu \Delta_N^q, \quad (4.17)$$

where s^μ is the spin of the nucleon. Meanwhile, the matrix element of the SI scattering is,

$$\begin{aligned} f_N/m_N = & \sum_{u,d,s} f_{Tq} f_q + \sum_{u,d,s,c,b} \frac{3}{4} [q(2) + \bar{q}(2)] (g_q^{(1)} + g_q^{(2)}) \\ & - \frac{8\pi}{9\alpha_s} f_{TG} f_G + \frac{3}{4} G(2) (g_G^{(1)} + g_G^{(2)}), \end{aligned} \quad (4.18)$$

where m_N is the nucleon mass and f_{Tq} , f_{TG} , $q(2)$, $\bar{q}(2)$ and $G(2)$ are hadronic matrix elements

$$\langle N | m_q \bar{q} q | N \rangle = f_{Tq} m_N, \quad (4.19)$$

$$\langle N | G_{\mu\nu}^a G^{a\mu\nu} | N \rangle = -\frac{8\pi}{9\alpha_s} f_{TG} m_N, \quad (4.20)$$

$$\langle N | O_{q,\mu\nu}^{(2)} | N \rangle = \frac{1}{m_N} (p_\mu p_\nu - \frac{1}{4} m_N^2 g_{\mu\nu}) (q(2) + \bar{q}(2)), \quad (4.21)$$

$$\langle N | O_{G,\mu\nu}^{(2)} | N \rangle = \frac{1}{m_N} (p_\mu p_\nu - \frac{1}{4} m_N^2 g_{\mu\nu}) G(2). \quad (4.22)$$

Here p is the momentum of the nucleon.

With these conventions, the SD and SI cross sections can be written as,

$$\sigma_{\chi N}^{\text{SD}} = \frac{12\mu_N^2}{\pi} (f^{\text{SD}})^2, \quad \sigma_{\chi N}^{\text{SI}} = \frac{4\mu_N^2}{\pi} f_N^2, \quad (4.23)$$

where μ_N is the reduced mass of the nucleon and DM, i.e. $\mu_N = m_N m_\chi / (m_N + m_\chi)$. The SD scattering is dominated by the tree level interactions and the matching coefficient f_q^{SD} could be got at the leading order with the large mass expansion of the mediators $\phi_{1,2,d}$. The detail of the calculation could be found in Refs. [50, 52] and the results are,

$$f_u^{\text{SD}} = -\frac{y_u^2}{8} \left[\frac{\sin^2 \theta}{m_\chi^2 - m_1^2} + \frac{\cos^2 \theta}{m_\chi^2 - m_2^2} \right], \quad (4.24)$$

$$f_d^{\text{SD}} = -\frac{y_u^2}{8} \frac{1}{m_\chi^2 - M_2^2}. \quad (4.25)$$

While the leading order cross section for the SI scattering will vanish due to the Majorana nature of the DM, as a result, it is necessary to go beyond the leading order in order to estimate the rate of SI scattering. The matching coefficients f_q and $g_q^{(1)}$ could be got from

the next-to-leading order expansion of the mediator $\phi_{1,2,d}$ propagators, i.e.

$$f_u = \frac{y_u^2 \sin^2 \theta}{16} \frac{m_\chi}{(m_\chi^2 - m_1^2)^2} + \frac{y_u^2 \cos^2 \theta}{16} \frac{m_\chi}{(m_\chi^2 - m_2^2)^2}, \quad (4.26)$$

$$f_d = \frac{y_u^2}{16} \frac{m_\chi}{(m_\chi^2 - M_2^2)^2}, \quad (4.27)$$

$$g_u^{(1)} = \frac{y_u^2 \sin^2 \theta}{4} \frac{m_\chi}{(m_\chi^2 - m_1^2)^2} + \frac{y_u^2 \cos^2 \theta}{4} \frac{m_\chi}{(m_\chi^2 - m_2^2)^2}, \quad (4.28)$$

$$g_d^{(1)} = \frac{y_u^2}{4} \frac{m_\chi}{(m_\chi^2 - M_2^2)^2}. \quad (4.29)$$

It shows that the SI matching coefficients f_q and $g_q^{(1)}$ are suppressed by factor $1/(m^2 - m_\chi^2)$, with $m = m_{1,2}, M_2$ compared to the f_q^{SD} in the region of we are interested in, i.e. $m_\chi \ll m_{1,2}, M_2$.

The SI matching coefficients f_G and $g_G^{(1,2)}$ could be induced at the one loop and can be calculated by the usual Feynman diagrams with the help of the projection operators. Alternatively, one can also use the Fock-Schwinger gauge to simplify the calculation [52, 64, 66], i.e. $x^\mu A_\mu = 0$. In this work, we will focus on the Fock-Schwinger gauge method and refer the reader to Ref. [52] for the detail of projection operator approach. In the Fock-Schwinger gauge, one can express the gluon field in terms of its field strength tensor $G_{\mu\nu}$ and maintain explicit gauge invariance for each step in the calculation. The Wilson coefficients can be extracted from the one loop correction to a Majorana fermion propagator through a non-zero background of gluon fields and it shows

$$\begin{aligned} f_G = & \frac{\alpha_s}{32\pi} \left\{ y_t^2 m_t^2 \left[\int \frac{d^4 q}{i\pi^2} \frac{(\not{p} + \not{q}) \cos^2 \theta}{(q^2 - m_1^2)[(p+q)^2 - m_t^2]^4} + \int \frac{d^4 q}{i\pi^2} \frac{(\not{p} + \not{q}) \sin^2 \theta}{(q^2 - m_2^2)[(p+q)^2 - m_t^2]^4} \right] \right. \\ & + y_t^2 m_1^2 \int \frac{d^4 q}{i\pi^2} \frac{(\not{p} + \not{q}) \cos^2 \theta}{[(q^2 - m_1^2)]^4 [(p+q)^2 - m_t^2]} + y_t^2 m_2^2 \int \frac{d^4 q}{i\pi^2} \frac{(\not{p} + \not{q}) \sin^2 \theta}{[(q^2 - m_2^2)]^4 [(p+q)^2 - m_t^2]} \\ & + y_u^2 m_1^2 \int \frac{d^4 q}{i\pi^2} \frac{(\not{p} + \not{q}) \sin^2 \theta}{[(q^2 - m_1^2)]^4 (p+q)^2} + y_u^2 m_2^2 \int \frac{d^4 q}{i\pi^2} \frac{(\not{p} + \not{q}) \cos^2 \theta}{[(q^2 - m_2^2)]^4 (p+q)^2} \\ & \left. + y_u^2 M_2^2 \int \frac{d^4 q}{i\pi^2} \frac{\not{p} + \not{q}}{[(q^2 - M_2^2)]^4 (p+q)^2} \right\}. \quad (4.30) \end{aligned}$$

The loop integration in Eq. 4.30 can be calculated analytically and we show the detail in the Appendix.

The Wilson coefficients of gluon twist-2 operators could be obtained from the scattering matrix element,

$$\begin{aligned} M_{\text{twist-2}} = & 2\pi\alpha_s \bar{\chi} [f(y_t \cos \theta, m_t, m_1) + f(y_t \sin \theta, m_t, m_2) + f(y_u \sin \theta, 0, m_1) \\ & + f(y_u \cos \theta, 0, m_2) + f(y_u, 0, M_2)] \chi O_{G,\mu\nu}^{(2)} \quad (4.31) \end{aligned}$$

where the function $f(g_\chi, m_q, m_\phi)$ is defined as,

$$\begin{aligned}
f(g_\chi, m_q, m_\phi) &= g_\chi^2 \int \frac{d^4 q}{(2\pi)^2} \frac{(\not{p} + \not{q})[-m_q^2 g^{\mu\nu} - 2(p+q)^\mu (p+q)^\nu]}{(q^2 - m_\phi^2)[(p+q)^2 - m_q^2]^4} \\
&+ g_\chi^2 \int \frac{d^4 q}{(2\pi)^2} \frac{\gamma^\mu (p+q)^\nu + \gamma^\nu (p+q)^\mu}{(q^2 - m_\phi^2)[(p+q)^2 - m_q^2]^3} \\
&+ \frac{1}{2} g_\chi^2 \int \frac{d^4 q}{(2\pi)^2} \frac{(\not{p} + \not{q})[(q^2 - m_\phi^2)g^{\mu\nu} - 4q^\mu q^\nu]}{(q^2 - m_\phi^2)^4[(p+q)^2 - m_q^2]}. \tag{4.32}
\end{aligned}$$

Therefore, the twist-2 Wilson coefficients are,

$$\begin{aligned}
g_G^{(1)} &= -\frac{\alpha_s}{96\pi m_\chi^3 \Delta} \left[g_1(y_t \cos \theta, m_t, m_1) + g_1(y_t \sin \theta, m_t, m_2) + g_1(y_u \sin \theta, 0, m_1) \right. \\
&\left. + g_1(y_u \cos \theta, 0, m_2) + g_1(y_u, 0, M_2) \right], \tag{4.33}
\end{aligned}$$

$$\begin{aligned}
g_G^{(2)} &= \frac{\alpha_s}{48\pi m_\chi^3 \Delta^2} \left[g_2(y_t \cos \theta, m_t, m_1) + g_2(y_t \sin \theta, m_t, m_2) + g_2(y_u \sin \theta, 0, m_1) \right. \\
&\left. + g_2(y_u \cos \theta, 0, m_2) + g_2(y_u, 0, M_2) \right], \tag{4.34}
\end{aligned}$$

where

$$\begin{aligned}
g_1(g_\chi, m_q, m_\phi) &= g_\chi^2 \left\{ [5m_\chi^4 m_q^2 + m_\chi^4 m_\phi^2 - 3m_\chi^2 m_q^4 + 3m_\chi^2 m_\phi^4 + (m_q^2 - m_\phi^2)^3 - 3m_\chi^6] L \right. \\
&\left. - 6m_\chi^4 + 2m_\chi^2 (m_q^2 - m_\phi^2) + \Delta \ln \frac{m_q^2}{m_\phi^2} \right\}, \tag{4.35}
\end{aligned}$$

$$\begin{aligned}
g_2(g_\chi, m_q, m_\phi) &= g_\chi^2 \left\{ [m_\chi^8 (m_q^2 - 5m_\phi^2) + 2m_\chi^6 (2m_q^2 m_\phi^2 - 4m_q^4 + 5m_\phi^4) + 10m_\chi^4 (m_q^6 - m_\phi^6) \right. \\
&- 5m_\chi^2 (m_q^2 - m_\phi^2)^3 (m_q^2 + m_\phi^2) + (m_q^2 - m_\phi^2)^5 + m_\chi^{10}] L + 2m_\chi^6 (m_q^2 - 4m_\phi^2) + \\
&\left. 7m_\chi^4 (m_\phi^4 - m_q^4) + 2m_\chi^2 (m_q^2 - m_\phi^2)^3 + 3m_\chi^8 + \Delta^2 \ln \frac{m_\phi^2}{m_q^2} \right\}. \tag{4.36}
\end{aligned}$$

The definition of Δ and L could be found in the Appendix; see Eqs. A.5 and A.6.

Next, we perform a numerical calculation for $\sigma_{\chi N}^{\text{SD}}$ and $\sigma_{\chi N}^{\text{SI}}$. The hadronic matrix elements are given by [67],

$$f_{Tu}^p = 0.018, \quad f_{Td}^p = 0.030, \quad f_{Tu}^n = 0.015, \quad f_{Td}^n = 0.034, \quad f_{TG} = 0.80. \tag{4.37}$$

Here f_{Tq}^N corresponds to the contribution of the quark q to the nucleon matrix elements for the nucleon N . The matrix elements of the twist-2 operators are related to the second moments of the parton distribution functions (PDFs),

$$q(2) + \bar{q}(2) = \int_0^1 dx x (q(x) + \bar{q}(x)), \quad G(2) = \int_0^1 dx x g(x), \tag{4.38}$$

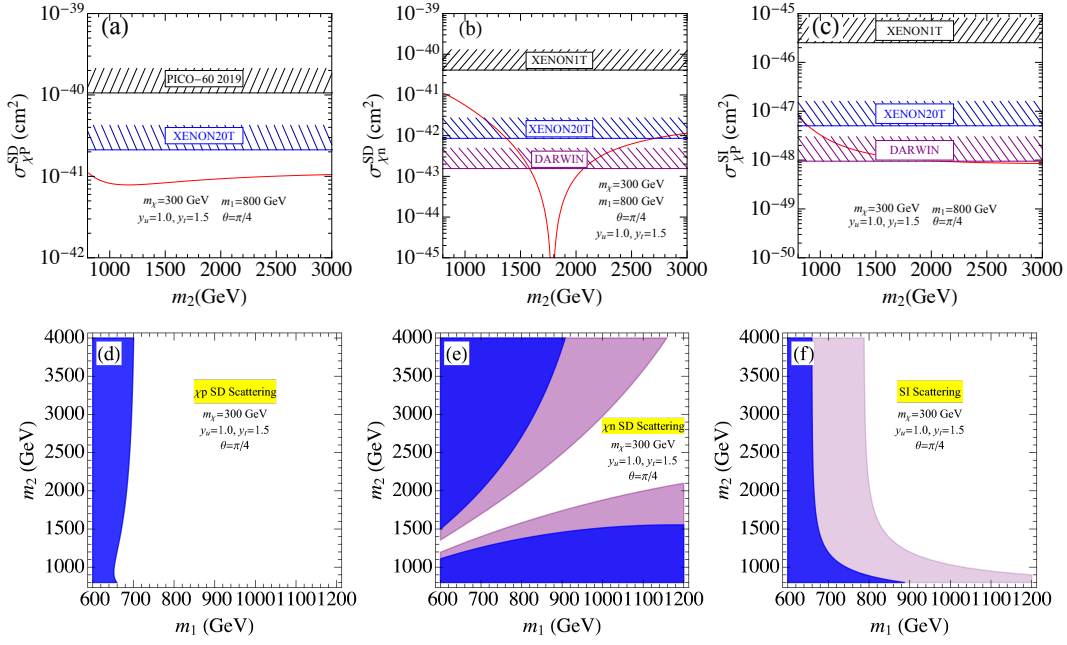


Figure 7. The constraints from DM direct detection experiments on the parameter m_2 (a,b,c) and m_1 - m_2 plane (d,e,f). The black meshed region denotes the limits from the current measurements PICO-60 and XENON1T, while the blue and purple meshed (shaded) regions are the bound from the future XENON20T and DARWIN, respectively.

where $q(x)$, $\bar{q}(x)$ and $g(x)$ are the PDFs of quark, anti-quark and gluon in nucleon N , respectively. Those hadronic elements could be extracted from the CT14NNLO PDFs [68],

$$[u(2) + \bar{u}(2)]_p = 0.3481, \quad [d(2) + \bar{d}(2)]_p = 0.1902, \quad G(2)_p = G(2)_n = 0.4159. \quad (4.39)$$

For the spin dependent matrix elements, we utilize the values in Ref. [69],

$$\Delta_p^u = 0.84, \quad \Delta_p^d = -0.43, \quad \Delta_n^u = -0.43, \quad \Delta_n^d = 0.84. \quad (4.40)$$

We show the DM SD and SI scattering rates with the benchmark parameters $m_\chi = 300$ GeV, $m_1 = 800$ GeV, $y_u = 1$, $y_t = 1.5$ and $\theta = \pi/4$ in Figs. 7(a)-(c) (red lines). The most severe limits for the SD scattering with proton and neutron targets are from PICO-60 [70] and XENON1T [71], respectively, and the upper limits are roughly $\mathcal{O}(10^{-40}\text{cm}^2)$ (black meshed regions). The SI scattering measurement from XENON1T could give a stronger bound for the cross section [71] (black meshed region), i.e. $\sigma_{\chi p}^{\text{SI}} \sim 10^{-45}\text{cm}^2$. While the expected constraints from XENON20T [46] (blue regions) and DARWIN [47] (purple region) could be further improved as compared to the present data and it shows the sensitivity could be enhanced about one to two order of magnitude for both the SD and SI scattering. We observe that the predictions from our model are consistent with the current measurements and also could be tested in the future experiments. In addition, we note that the cancellation between

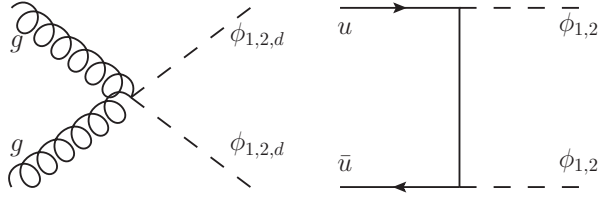


Figure 8. Illustrative Feynman diagrams of colored scalar pair production at the LHC.

up and down quarks' contributions in DM-neutron SD scattering will obviously change the cross section compared to the DM-proton SD process; see Fig. 7(b) (red lines). In Figs. 7(d)-(f), we show the expected sensitivity regions from the future XENON20T and DARWIN experiments on the plane of m_1 and m_2 . It is clear that both the DM-neutron SD and SI scattering could give a strong constraint for our simplified model and the measurements could probe complementary regions in the parameter space.

5 Direct Search at the LHC

In this section we discuss the constraints from LHC to our simplified model. The processes of interests to us include pair production of the colored mediators (ϕ_i , with $i = 1, 2, d$) and the associated production of mediators with DM. It has been shown that the second process plays a subdominant effects to constrain the model parameter space, and will be neglected from here on [52]. The pair of mediators could be produced through the strong force and the Yukawa interactions; see Fig. 8. We could use the null results from squark searches at the LHC to estimate the limits for our simplified model [72].

From the discussion of the top quark FCNC in Sec. 3, $m_1 \ll m_{d,2}$ is required in order to generate a sizable top quark FCNC signal at the LHC. As a consequence, the cross section of ϕ_i pair production would be determined by m_1 and the contributions from $\phi_{2,d}$ could be ignored. We consider separately the two decay channels $\phi_1 \rightarrow \chi u$ and $\phi_1 \rightarrow \chi t$ in the analysis. The branching ratios in these channels are depending on the Yukawa couplings $y_{u,t}$ and the mass splitting between ϕ_1 and χ . The signal events are characterized by multiple jets or top quarks and large missing transverse momentum. Both of them have been searched by ATLAS and CMS collaborations [72–75] and it shows that the bounds from the top quark is much weaker than the multiple jets final states in most parameter space [72]. Therefore, it would be a good approximation to use $pp \rightarrow \phi_1 \phi_1^* \rightarrow \chi \chi u \bar{u}$ channel to estimate the limits from LHC.

We use MadGraph5 [76] to generate the parton level events at 13 TeV and pass them to PYTHIA [77] for showering and hadroniation. The Delphes package is used to simulate the detector smearing effects [78]. Following the analysis strategy of CMS collaboration [72], we require the following kinematic cuts:

$$n_j = 2 \sim 3, \quad n_b = 0, \quad |\eta^j| < 2.4, \quad p_T^j > 30 \text{ GeV}, \quad H_T > p_T^{\text{miss}} > 300 \text{ GeV}, \quad (5.1)$$

$$\Delta\phi(\vec{p}_T^{\text{miss}}, j_1) > 0.5, \quad \Delta\phi(\vec{p}_T^{\text{miss}}, j_2) > 0.5, \quad \Delta\phi(\vec{p}_T^{\text{miss}}, j_3) > 0.3, \quad (5.2)$$

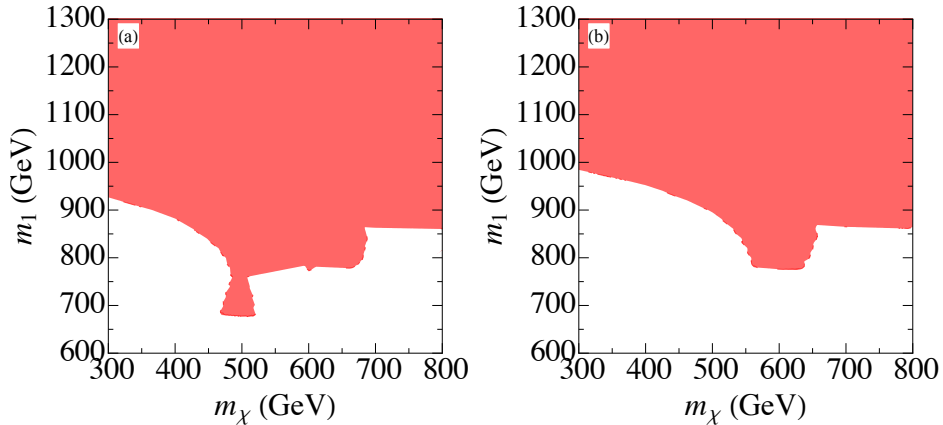


Figure 9. Parameter space allowed at the 13 TeV LHC with the integrated luminosity of 137 fb^{-1} at 95% C.L. on the plane of m_χ and m_1 for the benchmark parameters $y_u = 1.0$, $y_t = 1.5$ and $\theta = \pi/4$. (a) the contribution from ϕ_1 alone; (b) the contribution from ϕ_1 and ϕ_d with the assumption $m_1 = 0.8m_d$.

where $n_{j(b)}$ is the light (bottom) jet number, H_T is the scalar p_T sum of jets with $|\eta^j| < 2.4$ and p_T^{miss} is the missing transverse momentum. The search is performed in a four-dimensional region defined by exclusive intervals in n_j , n_b , H_T and p_T^{miss} . Based on the signal features of our model, we fix n_j and n_b in the analysis, while including the 10 kinematic intervals of H_T and p_T^{miss} which are defined in Ref. [72]. The significance for each bin q_{EL} could be estimated by the likelihood method and it shows

$$q_{\text{EL}} = \sqrt{-2 \left[N_{\text{Exp}} \ln \frac{N_s + N_b}{N_b} - N_s \right]}, \quad (5.3)$$

where N_{Exp} , N_s and N_b denote the number of observed, signal and SM background events, respectively. The N_{Exp} and N_b for each bin can be found in Ref. [72] and the systematic uncertainties for the background will be ignored in this analysis. The total significance for the 10 bins could be obtained by square root sum for each bin. Figure 9(a) shows the allowed parameter space on the plane of m_χ and m_1 at the 95% C.L. with the integrated luminosity of 137 fb^{-1} . In Fig. 9(b), we include the impact of the scalar ϕ_d with a benchmark parameter $m_1 = 0.8m_d$. It shows that the contribution from ϕ_d will only change the bound of m_1 slightly. Therefore, we expect the contributions from $\phi_{d,2}$ could be ignored in the parameter space of we are interested in, i.e. $m_1 \ll m_{d,2}$.

6 Conclusion

Due to the large hierarchy between the top quark FCNC anomalous couplings and the SM top quark interactions, it is well motivated to study the loop induced top quark FCNC processes at the LHC, which could avoid the possible unduly small NP couplings in the model. In this work, we consider one class of the simplified model which could only generate the top quark

FCNC couplings in the loop level. Such scenario predicts a Majorana dark matter candidate and could be tested through the scattering between dark matter and nuclei, and also the data from LHC.

In our simplified model, the top quark could decay to $q+Z/\gamma/g/h$ and the most promising decay channel at the HL-LHC and future hadron colliders would be $t \rightarrow qh$. Its branching ratio is around $\mathcal{O}(10^{-5})$ in some parameter space. Comparing to the expected limits from the HL-LHC, the unitarity band from $\phi\phi \rightarrow W_L W_L$ scattering would give a stronger constraint for the model parameters.

To full explore the discovery potential of our simplified model, we carried out a comprehensive comparison of the dark matter relic density, direct detection experiments and LHC searches. Due to the Majorana nature of the dark matter in our model, we note that the SI scattering with nuclei at leading order will vanish, while it could be generated at the next-to-leading order. Although the SI cross section from higher order will be suppressed compared to the tree level SD case, the SI scattering also provides a comparable limits to the SD production. Our analysis shows that the simplified model could easily satisfy the relic density limits, while the direct detection experiments from the scattering between dark matter and nuclei and LHC searches provide the severe bounds. In particular, the constraints from scattering between dark matter and neutron. When comparing the direct detection experiments and LHC searches, we note that they could probe complementary and same regions in parameter space, and are both necessary to fully constrain our simplified model.

Acknowledgments

We thank Qing-Hong Cao, Zhaofeng Kang, Jue Zhang and Ya Zhang for helpful discussions. The work of Y. Liu is supported in part by the National Science Foundation of China under Grant Nos. 11805013, 12075257 and the Fundamental Research Funds for the Central Universities under Grant No. 2018NTST09, BY is supported by the U.S. Department of Energy, Office of Science, Office of Nuclear Physics, under Contract DE-AC52-06NA25396, [under an Early Career Research Award (C. Lee),] and through the LANL/LDRD Program, RZ is supported in part by the National Science Foundation of China under Grant Nos. 12075257 and the funding from the Institute of High Energy Physics, Chinese Academy of Sciences (Y6515580U1) and the funding from Chinese Academy of Sciences (Y8291120K2)

A Feynman Integral

In the appendix we represent the details of the Feynman integrals in Eq. 4.30,

$$\int \frac{d^4 q}{i\pi^2} \frac{(\not{p} + \not{q})}{(q^2 - m_\phi^2)[(p+q)^2 - m_q^2]^4}, \quad (\text{A.1})$$

and

$$\int \frac{d^4 q}{i\pi^2} \frac{(\not{p} + \not{q})}{(q^2 - m_\phi^2)^4[(p+q)^2 - m_q^2]}. \quad (\text{A.2})$$

Note we can substitute \not{p} with m_χ in terms of Dirac equation of dark matter field with momentum p . Utilizing the Feynman parametrization method, we obtain

$$\begin{aligned} & \int \frac{d^4q}{i\pi^2} \frac{(\not{p} + \not{q})}{(q^2 - m_\phi^2)[(p+q)^2 - m_q^2]^4} \\ &= \frac{6m_q^2 m_\phi^2 (m_\phi^2 + m_q^2 - m_\chi^2)L + \Delta - 12m_q^2 m_\phi^2}{6m_q^2 \Delta^2}, \end{aligned} \quad (\text{A.3})$$

and

$$\begin{aligned} & \int \frac{d^4q}{i\pi^2} \frac{(\not{p} + \not{q})}{(q^2 - m_\phi^2)^4 [(p+q)^2 - m_q^2]} \\ &= \frac{(\Delta + 6m_\phi^2 m_q^2)(m_\phi^2 + m_q^2 - m_\chi^2) - 12m_q^4 m_\phi^4 L}{6m_\phi^4 \Delta^2}, \end{aligned} \quad (\text{A.4})$$

where the symbols Δ and L are defined as

$$\Delta = 4m_\phi^2 m_\chi^2 - (m_q^2 - m_\chi^2 - m_\phi^2)^2, \quad (\text{A.5})$$

and

$$L = \begin{cases} \frac{2}{\sqrt{|\Delta|}} \tanh^{-1} \frac{\sqrt{|\Delta|}}{m_q^2 + m_\phi^2 - m_\chi^2}, & \Delta < 0 \\ \frac{4m_\chi^2}{m_q^4 + m_\phi^4 - m_\chi^4 - 2m_q^2 m_\phi^2}, & \Delta = 0 \\ \frac{2}{\sqrt{\Delta}} \tan^{-1} \frac{\sqrt{\Delta}}{m_q^2 + m_\phi^2 - m_\chi^2}. & \Delta > 0 \end{cases}. \quad (\text{A.6})$$

References

- [1] S. L. Glashow, J. Iliopoulos, and L. Maiani, *Weak Interactions with Lepton-Hadron Symmetry*, Phys. Rev. **D2** (1970) 1285–1292.
- [2] J. Aguilar-Saavedra, *Top flavor-changing neutral interactions: Theoretical expectations and experimental detection*, Acta Phys. Polon. B **35** (2004) 2695–2710, [[hep-ph/0409342](#)].
- [3] R. Gaitán, J. H. Montes de Oca, E. A. Garcés, and R. Martínez, *Rare top decay $t \rightarrow c\gamma$ with flavor changing neutral scalar interactions in two Higgs doublet model*, Phys. Rev. **D94** (2016), no. 9 094038, [[arXiv:1503.04391](#)].
- [4] G. Abbas, A. Celis, X.-Q. Li, J. Lu, and A. Pich, *Flavour-changing top decays in the aligned two-Higgs-doublet model*, JHEP **06** (2015) 005, [[arXiv:1503.06423](#)].
- [5] A. Arhrib, R. Benbrik, C.-H. Chen, M. Gomez-Bock, and S. Semmlali, *Two-Higgs-doublet type-II and -III models and $t \rightarrow ch$ at the LHC*, Eur. Phys. J. **C76** (2016), no. 6 328, [[arXiv:1508.06490](#)].
- [6] K. Y. Oyulmaz, A. Senol, H. Denizli, A. Yilmaz, I. Turk Cakir, and O. Cakir, *Probing anomalous $tq\gamma$ and tqg couplings via single top production in association with photon at FCC-hh*, Eur. Phys. J. C **79** (2019), no. 1 83, [[arXiv:1811.01074](#)].

- [7] L. Shi and C. Zhang, *Probing the top quark flavor-changing couplings at CEPC*, Chin. Phys. C **43** (2019), no. 11 113104, [[arXiv:1906.04573](#)].
- [8] H. Khanpour, *Probing top quark FCNC couplings in the triple-top signal at the high energy LHC and future circular collider*, Nucl. Phys. B **958** (2020) 115141, [[arXiv:1909.03998](#)].
- [9] J.-j. Cao, G.-l. Liu, J. M. Yang, and H.-j. Zhang, *Top-quark FCNC Productions at CERN LHC in Topcolor-assisted Technicolor Model*, Phys. Rev. **D76** (2007) 014004, [[hep-ph/0703308](#)].
- [10] J. M. Yang, *Probing New Physics from Top Quark FCNC Processes at LHC: A Mini Review*, Int. J. Mod. Phys. **A23** (2008) 3343–3347, [[arXiv:0801.0210](#)].
- [11] J. J. Zhang, C. S. Li, J. Gao, H. Zhang, Z. Li, C. P. Yuan, and T.-C. Yuan, *Next-to-leading order QCD corrections to the top quark decay via model-independent FCNC couplings*, Phys. Rev. Lett. **102** (2009) 072001, [[arXiv:0810.3889](#)].
- [12] X.-F. Han, L. Wang, and J. M. Yang, *Top quark FCNC decays and productions at LHC in littlest Higgs model with T-parity*, Phys. Rev. **D80** (2009) 015018, [[arXiv:0903.5491](#)].
- [13] C.-X. Yue, J. Wang, Y. Yu, and T.-T. Zhang, *The anomalous top quark coupling tqg and tW production at the LHC*, Phys. Lett. **B705** (2011) 222–227, [[arXiv:1105.5227](#)].
- [14] J. Gao, C. S. Li, L. L. Yang, and H. Zhang, *Search for anomalous top quark production at the early LHC*, Phys. Rev. Lett. **107** (2011) 092002, [[arXiv:1104.4945](#)].
- [15] J. Cao, C. Han, L. Wu, J. M. Yang, and M. Zhang, *SUSY induced top quark FCNC decay $t \rightarrow ch$ after Run I of LHC*, Eur. Phys. J. **C74** (2014), no. 9 3058, [[arXiv:1404.1241](#)].
- [16] H. Sun, *Probe anomalous $tq\gamma$ couplings through single top photoproduction at the LHC*, Nucl. Phys. **B886** (2014) 691–711, [[arXiv:1402.1817](#)].
- [17] W. Liu, H. Sun, X. Wang, and X. Luo, *Probing the anomalous FCNC top-Higgs Yukawa couplings at the Large Hadron Electron Collider*, Phys. Rev. **D92** (2015), no. 7 074015, [[arXiv:1507.03264](#)].
- [18] H. Sun and X. Wang, *Exploring the Anomalous Top-Higgs FCNC Couplings at the electron proton colliders*, Eur. Phys. J. **C78** (2018), no. 4 281, [[arXiv:1602.04670](#)].
- [19] X. Wang, H. Sun, and X. Luo, *Searches for the Anomalous FCNC Top-Higgs Couplings with Polarized Electron Beam at the LHeC*, Adv. High Energy Phys. **2017** (2017) 4693213, [[arXiv:1703.02691](#)].
- [20] CMS Collaboration, V. Khachatryan et al., *Search for Anomalous Single Top Quark Production in Association with a Photon in pp Collisions at $\sqrt{s} = 8$ TeV*, JHEP **04** (2016) 035, [[arXiv:1511.03951](#)].
- [21] ATLAS Collaboration, G. Aad et al., *Search for flavour-changing neutral currents in processes with one top quark and a photon using 81 fb^{-1} of pp collisions at $\sqrt{s} = 13$ TeV with the ATLAS experiment*, Phys. Lett. B **800** (2020) 135082, [[arXiv:1908.08461](#)].
- [22] CDF Collaboration, F. Abe et al., *Search for flavor-changing neutral current decays of the top quark in $p\bar{p}$ collisions at $\sqrt{s} = 1.8$ TeV*, Phys. Rev. Lett. **80** (1998) 2525–2530.
- [23] CMS Collaboration, V. Khachatryan et al., *Search for anomalous Wtb couplings and flavour-changing neutral currents in t -channel single top quark production in pp collisions at $\sqrt{s} = 7$ and 8 TeV*, JHEP **02** (2017) 028, [[arXiv:1610.03545](#)].

- [24] **ATLAS** Collaboration, G. Aad et al., *Search for single top-quark production via flavour-changing neutral currents at 8 TeV with the ATLAS detector*, Eur. Phys. J. **C76** (2016), no. 2 55, [[arXiv:1509.00294](#)].
- [25] **CDF** Collaboration, T. Aaltonen et al., *Search for top-quark production via flavor-changing neutral currents in $W+1$ jet events at CDF*, Phys. Rev. Lett. **102** (2009) 151801, [[arXiv:0812.3400](#)].
- [26] **DO** Collaboration, V. M. Abazov et al., *Search for Flavor Changing Neutral Currents via Quark-Gluon Couplings in Single Top Quark Production using 2.3 fb^{-1} of $p\bar{p}$ Collisions*, Phys. Lett. B **693** (2010) 81–87, [[arXiv:1006.3575](#)].
- [27] **CMS** Collaboration, S. Chatrchyan et al., *Search for Flavor-Changing Neutral Currents in Top-Quark Decays $t \rightarrow Zq$ in pp Collisions at $\sqrt{s} = 8 \text{ TeV}$* , Phys. Rev. Lett. **112** (2014), no. 17 171802, [[arXiv:1312.4194](#)].
- [28] **CMS** Collaboration, A. M. Sirunyan et al., *Search for associated production of a Z boson with a single top quark and for tZ flavour-changing interactions in pp collisions at $\sqrt{s} = 8 \text{ TeV}$* , JHEP **07** (2017) 003, [[arXiv:1702.01404](#)].
- [29] **ATLAS** Collaboration, M. Aaboud et al., *Search for flavour-changing neutral current top-quark decays $t \rightarrow qZ$ in proton-proton collisions at $\sqrt{s} = 13 \text{ TeV}$ with the ATLAS detector*, JHEP **07** (2018) 176, [[arXiv:1803.09923](#)].
- [30] **ATLAS** Collaboration, G. Aad et al., *Search for flavour-changing neutral current top-quark decays to qZ in pp collision data collected with the ATLAS detector at $\sqrt{s} = 8 \text{ TeV}$* , Eur. Phys. J. C **76** (2016), no. 1 12, [[arXiv:1508.05796](#)].
- [31] **CDF** Collaboration, T. Aaltonen et al., *Search for the Flavor Changing Neutral Current Decay $t \rightarrow Zq$ in $p\bar{p}$ Collisions at $\sqrt{s} = 1.96 \text{ TeV}$* , Phys. Rev. Lett. **101** (2008) 192002, [[arXiv:0805.2109](#)].
- [32] **DO** Collaboration, V. M. Abazov et al., *Search for Flavor Changing Neutral Currents in Decays of Top Quarks*, Phys. Lett. B **701** (2011) 313–320, [[arXiv:1103.4574](#)].
- [33] **CMS** Collaboration, V. Khachatryan et al., *Search for top quark decays via Higgs-boson-mediated flavor-changing neutral currents in pp collisions at $\sqrt{s} = 8 \text{ TeV}$* , JHEP **02** (2017) 079, [[arXiv:1610.04857](#)].
- [34] **CMS** Collaboration, A. M. Sirunyan et al., *Search for the flavor-changing neutral current interactions of the top quark and the Higgs boson which decays into a pair of b quarks at $\sqrt{s} = 13 \text{ TeV}$* , JHEP **06** (2018) 102, [[arXiv:1712.02399](#)].
- [35] **ATLAS** Collaboration, M. Aaboud et al., *Search for top-quark decays $t \rightarrow Hq$ with 36 fb^{-1} of pp collision data at $\sqrt{s} = 13 \text{ TeV}$ with the ATLAS detector*, JHEP **05** (2019) 123, [[arXiv:1812.11568](#)].
- [36] L. Lavoura, *General formulae for $f(1) \rightarrow f(2)$ gamma*, Eur. Phys. J. **C29** (2003) 191–195, [[hep-ph/0302221](#)].
- [37] C. Degrande, F. Maltoni, J. Wang, and C. Zhang, *Automatic computations at next-to-leading order in QCD for top-quark flavor-changing neutral processes*, Phys. Rev. **D91** (2015) 034024, [[arXiv:1412.5594](#)].

- [38] G. Durieux, F. Maltoni, and C. Zhang, *Global approach to top-quark flavor-changing interactions*, Phys. Rev. **D91** (2015), no. 7 074017, [[arXiv:1412.7166](#)].
- [39] S. L. Glashow and S. Weinberg, *Natural Conservation Laws for Neutral Currents*, Phys. Rev. **D15** (1977) 1958.
- [40] E. A. Paschos, *Diagonal Neutral Currents*, Phys. Rev. **D15** (1977) 1966.
- [41] Q.-H. Cao, B. Yan, J.-H. Yu, and C. Zhang, *A General Analysis of Wtb anomalous Couplings*, Chin. Phys. C **41** (2017), no. 6 063101, [[arXiv:1504.03785](#)].
- [42] Q.-H. Cao and B. Yan, *Determining V_{tb} at electron-positron colliders*, Phys. Rev. D **92** (2015), no. 9 094018, [[arXiv:1507.06204](#)].
- [43] Q.-H. Cao, B. Yan, C. Yuan, and Y. Zhang, *Probing $Zt\bar{t}$ couplings using Z boson polarization in ZZ production at hadron colliders*, Phys. Rev. D **102** (2020), no. 5 055010, [[arXiv:2004.02031](#)].
- [44] E. Ma, *Pathways to naturally small neutrino masses*, Phys. Rev. Lett. **81** (1998) 1171–1174, [[hep-ph/9805219](#)].
- [45] Q.-H. Cao, S.-L. Chen, E. Ma, B. Yan, and D.-M. Zhang, *New Class of Two-Loop Neutrino Mass Models with Distinguishable Phenomenology*, Phys. Lett. B **779** (2018) 430–435, [[arXiv:1707.05896](#)].
- [46] **XENON** Collaboration, E. Aprile et al., *Projected WIMP sensitivity of the XENONnT dark matter experiment*, JCAP **2011** (2020) 031, [[arXiv:2007.08796](#)].
- [47] **DARWIN** Collaboration, J. Aalbers et al., *DARWIN: towards the ultimate dark matter detector*, JCAP **1611** (2016) 017, [[arXiv:1606.07001](#)].
- [48] M. Blanke and S. Kast, *Top-Flavoured Dark Matter in Dark Minimal Flavour Violation*, JHEP **05** (2017) 162, [[arXiv:1702.08457](#)].
- [49] M. Blanke, S. Das, and S. Kast, *Flavoured Dark Matter Moving Left*, JHEP **02** (2018) 105, [[arXiv:1711.10493](#)].
- [50] A. DiFranzo, K. I. Nagao, A. Rajaraman, and T. M. P. Tait, *Simplified Models for Dark Matter Interacting with Quarks*, JHEP **11** (2013) 014, [[arXiv:1308.2679](#)]. [Erratum: JHEP 01, 162 (2014)].
- [51] C. Kilic, M. D. Klimek, and J.-H. Yu, *Signatures of Top Flavored Dark Matter*, Phys. Rev. **D91** (2015), no. 5 054036, [[arXiv:1501.02202](#)].
- [52] K. A. Mohan, D. Sengupta, T. M. P. Tait, B. Yan, and C. P. Yuan, *Direct Detection and LHC constraints on a t -Channel Simplified Model of Majorana Dark Matter at One Loop*, JHEP **05** (2019) 115, [[arXiv:1903.05650](#)].
- [53] G. 't Hooft and M. J. G. Veltman, *Scalar One Loop Integrals*, Nucl. Phys. **B153** (1979) 365–401.
- [54] **CMS** Collaboration, CMS, *Prospects for the search for gluon-mediated FCNC in top quark production with the CMS Phase-2 detector at the HL-LHC*, **CMS-PAS-FTR-18-004**.
- [55] T. Hahn and M. Perez-Victoria, *Automatized one loop calculations in four-dimensions and D -dimensions*, Comput. Phys. Commun. **118** (1999) 153–165, [[hep-ph/9807565](#)].

- [56] ATLAS, *Sensitivity of ATLAS at HL-LHC to flavour changing neutral currents in top quark decays $t \rightarrow cH$, with $H \rightarrow \gamma\gamma$* , [ATL-PHYS-PUB-2013-012](#).
- [57] ATLAS, *Expected sensitivity of ATLAS to FCNC top quark decays $t \rightarrow Zq$ and $t \rightarrow Hq$ at the High Luminosity LHC*, [ATL-PHYS-PUB-2016-019](#).
- [58] Y.-J. Zhang and J.-F. Shen, *Probing anomalous tqh couplings via single top production in associated with the Higgs boson at the HE-LHC and FCC-hh*, *Eur. Phys. J.* **C80** (2020), no. 9 811.
- [59] M. S. Chanowitz, M. A. Furman, and I. Hinchliffe, *Weak Interactions of Ultraheavy Fermions. 2.*, *Nucl. Phys.* **B153** (1979) 402–430.
- [60] B. W. Lee, C. Quigg, and H. B. Thacker, *The Strength of Weak Interactions at Very High-Energies and the Higgs Boson Mass*, *Phys. Rev. Lett.* **38** (1977) 883–885.
- [61] B. W. Lee, C. Quigg, and H. B. Thacker, *Weak Interactions at Very High-Energies: The Role of the Higgs Boson Mass*, *Phys. Rev.* **D16** (1977) 1519.
- [62] M. S. Chanowitz, M. A. Furman, and I. Hinchliffe, *Weak Interactions of Ultraheavy Fermions*, *Phys. Lett.* **78B** (1978) 285.
- [63] **Planck** Collaboration, N. Aghanim et al., *Planck 2018 results. VI. Cosmological parameters*, [arXiv:1807.06209](#).
- [64] J. Hisano, K. Ishiwata, and N. Nagata, *Gluon contribution to the dark matter direct detection*, *Phys. Rev. D* **82** (2010) 115007, [[arXiv:1007.2601](#)].
- [65] R. J. Hill and M. P. Solon, *Standard Model anatomy of WIMP dark matter direct detection I: weak-scale matching*, *Phys. Rev. D* **91** (2015) 043504, [[arXiv:1401.3339](#)].
- [66] V. A. Novikov, M. A. Shifman, A. I. Vainshtein, and V. I. Zakharov, *Calculations in External Fields in Quantum Chromodynamics. Technical Review*, *Fortsch. Phys.* **32** (1984) 585.
- [67] R. J. Hill and M. P. Solon, *Standard Model anatomy of WIMP dark matter direct detection II: QCD analysis and hadronic matrix elements*, *Phys. Rev. D* **91** (2015) 043505, [[arXiv:1409.8290](#)].
- [68] S. Dulat, T.-J. Hou, J. Gao, M. Guzzi, J. Huston, P. Nadolsky, J. Pumplin, C. Schmidt, D. Stump, and C. Yuan, *New parton distribution functions from a global analysis of quantum chromodynamics*, *Phys. Rev. D* **93** (2016), no. 3 033006, [[arXiv:1506.07443](#)].
- [69] M. Freytsis and Z. Ligeti, *On dark matter models with uniquely spin-dependent detection possibilities*, *Phys. Rev. D* **83** (2011) 115009, [[arXiv:1012.5317](#)].
- [70] **PICO** Collaboration, C. Amole et al., *Dark Matter Search Results from the Complete Exposure of the PICO-60 C_3F_8 Bubble Chamber*, *Phys. Rev.* **D100** (2019), no. 2 022001, [[arXiv:1902.04031](#)].
- [71] **XENON** Collaboration, E. Aprile et al., *Dark Matter Search Results from a One Ton-Year Exposure of XENON1T*, *Phys. Rev. Lett.* **121** (2018), no. 11 111302, [[arXiv:1805.12562](#)].
- [72] **CMS** Collaboration, A. M. Sirunyan et al., *Search for supersymmetry in proton-proton collisions at 13 TeV in final states with jets and missing transverse momentum*, *JHEP* **10** (2019) 244, [[arXiv:1908.04722](#)].

- [73] **ATLAS** Collaboration, G. Aad et al., *Search for squarks and gluinos in final states with jets and missing transverse momentum using 139 fb^{-1} of $\sqrt{s} = 13 \text{ TeV}$ pp collision data with the ATLAS detector*, [arXiv:2010.14293](#).
- [74] **ATLAS** Collaboration, G. Aad et al., *Search for a scalar partner of the top quark in the all-hadronic $t\bar{t}$ plus missing transverse momentum final state at $\sqrt{s} = 13 \text{ TeV}$ with the ATLAS detector*, Eur. Phys. J. C **80** (2020), no. 8 737, [[arXiv:2004.14060](#)].
- [75] **CMS** Collaboration, A. M. Sirunyan et al., *Search for top squark pair production using dilepton final states in pp collision data collected at $\sqrt{s} = 13 \text{ TeV}$* , Eur. Phys. J. C **81** (2021), no. 1 3, [[arXiv:2008.05936](#)].
- [76] J. Alwall, R. Frederix, S. Frixione, V. Hirschi, F. Maltoni, O. Mattelaer, H. S. Shao, T. Stelzer, P. Torrielli, and M. Zaro, *The automated computation of tree-level and next-to-leading order differential cross sections, and their matching to parton shower simulations*, JHEP **07** (2014) 079, [[arXiv:1405.0301](#)].
- [77] T. Sjöstrand, S. Ask, J. R. Christiansen, R. Corke, N. Desai, P. Ilten, S. Mrenna, S. Prestel, C. O. Rasmussen, and P. Z. Skands, *An introduction to PYTHIA 8.2*, Comput. Phys. Commun. **191** (2015) 159–177, [[arXiv:1410.3012](#)].
- [78] **DELPHES 3** Collaboration, J. de Favereau, C. Delaere, P. Demin, A. Giammanco, V. Lemaître, A. Mertens, and M. Selvaggi, *DELPHES 3, A modular framework for fast simulation of a generic collider experiment*, JHEP **02** (2014) 057, [[arXiv:1307.6346](#)].